U.Porto Journal of Engineering, 9:1 (2023) 55-71
ISSN 2183-6493
DOI: 10.24840/2183-6493_009-001_001134

Received: 24 November, 2022
Revised: 8 February, 2022
Published: 23 January, 2023

Analysis of skewing effects on radial force for different topologies of switched reluctance machines: 6/4 SRM, 8/6 SRM, and 12/8 SRM

Zeineb Touati[1], Rui Esteves Araújo[2], Imed Mahmoud[1], Adel Khedher[1]

[1]Université de Sousse, Ecole Nationale d'Ingénieurs de Sousse, LATIS-Laboratory of Advanced Technology and Intelligent Systems, 4023, Sousse, Tunisie; (zeineb.touati@eniso.u-sousse.tn), (mahmoud.imed@issatm.rnu.tn) , (adel.khedher@eniso.u-sousse.tn)

[2]INESC TEC and Faculty of Engineering, University of Porto, 4200-465 Porto, Portugal; (raraujo@fe.up.pt) ORCID 0000-0002-7866-9068

Abstract

Reducing vibration and noise in electrical machines for a given application is not a straightforward task, especially when the application imposes some restrictions. There are many techniques for reducing vibration based on design or control. Switched reluctance motors (SRMs) have a double-saliency structure, which results in a radial pulsation force. Consequently, they cause vibration and acoustic noise. This paper investigates the correlation between the radial force and the skew angle of the stator and/or rotor circuits. We computed the analysis from two-dimensional (2D) transient magnetic finite-element analysis (FEA) of three machine topologies, namely the 12/8 three-phase SRM, the 6/4 three-phase SRM and the 8/6 four-phase SRM. Compared to SRM, these topologies have the same basic dimensions (stator outer diameter, rotor outer diameter, and length) and operate in the same magnetic circuit saturation. The flux linkage and torque characteristics of the different motors are presented. The radial force distributed on the stator yoke under various skewing angles is studied extensively by FEA for the three machines. It is also demonstrated the effect of skewing angles in the reduction of radial force without any reduction in torque production.

Author Keywords. Finite element analysis, Switched reluctance machine, Skewing, Radial force, Vibration.

Type: Research Article
Open Access Peer Reviewed CC BY

1. Introduction

In industrial applications, the Switched Reluctance Machine (SRM) has attracted much interest. It is a good candidate for electric or hybrid vehicles (Cheng et al. 2019), (Fathabadi 2018), and (Martinez et al. 2016), electrical energy production (Bahy et al. 2020), (Chen et al. 2020), and (Dong et al. 2017), aeronautics (Bartolo et al. 2016) and flywheel energy storage systems (Cárdenas s et al. 2006). SRMs have several advantages, such as robust construction without windings or magnets on the rotor, high reliability, low manufacturing cost, high torque, insensitivity to high temperatures, and fault tolerance (Dias et al. 2020), (dos Santos Barros et al. 2017), (Sarr et al. 2020), and (Lu et al. 2020). SRMs are gaining popularity as a realizable alternative to synchronous reluctance machines (SynRM) and induction machines (IM). These machines have a common feature: they are robust and relatively insensitive to temperature due to the mechanical resilience of their rotors because of the absence of windings and permanent magnets. This robustness is achieved by reducing torque density and energy efficiency. However, there are major differences between them, and SRMs have salient

poles in both the stator and rotor and use concentrated windings. Last but not least, the low cost their manufacture can favor their use. The concentrated coils make SRMs more robust, but they are also in part responsible for their main drawback, the high torque ripple. The torque ripple in SRM compared to other types of machines is exceptionally high, which causes noise and vibration (Lin and Babak. 2013). In the field of SRM design, it is very known that the main sources of acoustic noise and vibration are the radial magnetic force and torque ripple. Therefore, for decades, researchers and engineers have focused on reducing the vibration and noise of this machine. For SRM, the attractive force can be distributed into tangential and radial forces. The tangential force is converted into rotating torque, while the radial force contributes to acoustic noise and vibration (Anwar et al. 2002). In (Lin and Babak. 2013), the origin of vibration in 8/6-pole SRMs is investigated, and a new method for the prediction of vibration is proposed. Most of these drawbacks can be mitigated by the development of control methods and/or geometry changes in its magnetic circuits. Accurate calculations of radial force and design of improved motor structures are the main routes for reducing SRM vibration (Somesan et al. 2013).

As far as the novelty is concerned, the main objective is to clarify the impact of the skewing methods in the SRM. Indeed, over the last years, few authors have discussed the problem of SRM performance in terms of skew methods. In (Li et al. 2008), the vibration and acoustic noise characteristics of the 12/8-pole and 6/4-pole SRMs are studied and compared. For example, in (Lin and Babak. 2013), a fast and precise method is developed for predicting acoustic noise, based on the spectrum distribution of radial vibration measured on the stator frame. In (Chun et al. 2015), a study of skewing the stator and/or rotor of 12/8-pole SRMs and their effect on the vibration reduction was done. Under different skewing angles, the force radial distributed on the stator yoke is investigated by a three-dimensional (3-D) finite element method (FEM). However, they have not studied other SRM topologies. A design methodology for an asymmetrical skew rotor-switched reluctance machine (ASR-SRM) using a multi-objective differential evolutionary (DE) algorithm in order to reduce torque ripple is presented in (Torres et al. 2021**)**. The authors in (Isfahani et al. 2014) compare the mechanical vibration between a double-stator switched reluctance machine and a conventional SRM. An electromagnetic FEA method is used to compute the acceleration, deformation, and velocity of the vibrating surface at a selected point on the outer surface of the machine. In (Gupta et al. 2021), the authors investigated the mitigation of the torque ripple by varying the SRM geometric parameters based on the FEA results. In (Ganji et al. 2015), a parametric electromagnetic model was developed for a Switched Reluctance Generator (SRG) with FEA, which could be considered appropriate for the accurate analysis and optimal design. Innovations on the design of 6x4 and 6x6 SRG were presented to increase the efficiency in (Dias et al. 2017).

Motivated by the mentioned issues, this work addresses the identified limitations via geometric design. First, three SRM motors are designed with a difference in the number of poles. Second, three different methods of skewing angles are analyzed and compared for different SRM topologies. In addition, despite the various studies we still do not have a definitive and categorical answer on what is the best geometric structure to attenuate the noise and vibrations of SRM. Therefore, this work is an effort to shed some light on the geometric effects. Thus, how can we maximize the SRM performance provided by skew methods? For that, this paper studies the radial force distributed on the stator yoke by developing different skewing methods. We compare and investigate the effect of skewed stator-SRM (SS-SRM), a skewed rotor-SRM (RS-SRM), and a skewed stator and rotor-SRM (RSS-

SRM) for different topologies of SRM, namely the 12/8 three-phase SRM, the 6/4 three-phase SRM and the 8/6 four-phase SRM. The radial force distributed on the stator yoke at various skewing angles is investigated by two-dimensional (2-D) finite element studies in MagNet software. In order to enrich this study, the flux linkage and torque characteristics of motor structures considered are also compared. In addition to the introduction and the conclusion, in section 2 the description of switched reluctance machines is presented. The study of skewing effects for the three motors are given in section 3.

2. Description of Switched Reluctance Machines

2.1. Machine Structures

Over the years, research has been based mainly on the design of an electric machine. SRM design is apparently similar to traditional machine designs, but they differ in several points due to the unique features of SRMs. Some characteristics simplify the design, such as the absence of coils and magnets in the rotor, the ability to operate over a wide speed range and the absence of brushes. Nevertheless, other characteristics such as inductance nonlinearity, excessive saturation for some rotor positions and complexity of the modeling SRM make it a complex process. SRM performance analysis, both electric and magnetic, depends on its geometric construction and materials used (Pushparajesh et al. 2019). It is almost impossible to determine the exact mathematical equations that take all these influential parameters into account (Pushparajesh et al. 2019). In this way, the main idea of this work is to develop a model that incorporates the influence of some parameters. Moreover, it can give useful results to calculate the electric machine's performance. **Figure 1** illustrates all the dimensions that must be determined for the construction of an SRM, where g is the length of the air gap, D_s is the outer diameter, D_r is the inner diameter, D_0 is the shaft diameter, β_r is the rotor pole arc, β_s is the stator pole arc, H_s is the stator pole height, H_r is the rotor pole height, Y_s is the stator back iron thickness, and Y_r is the rotor back iron thickness.

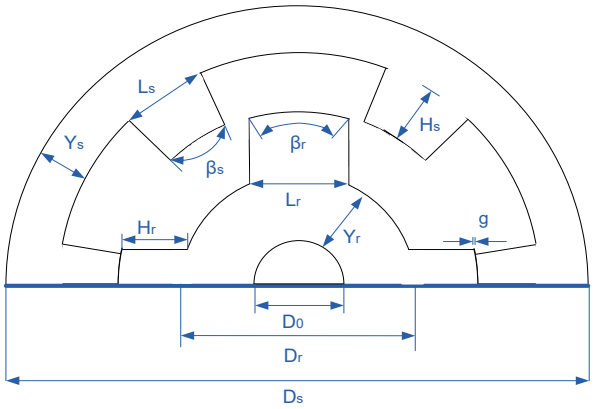

Figure 1: A portion of the magnetic circuit of a SRM to define the dimensions.

The conditions for the choice of stator and rotor pole angles can be represented graphically in a possibility triangle. The values of the polar arcs of the machine need to be within this triangle. **Figure 2** shows the possibility triangle for a 12/8 SRM, an 8/6 SRM and a 6/4 SRM.

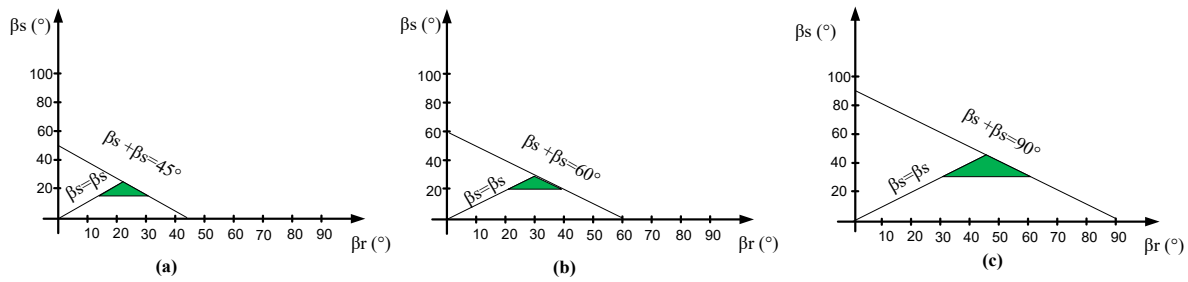

Figure 2: Limits of pole arcs: (a) Three-phase 12/8 SRM, (b) Four-phase 8/6 SRM and (c) Three-phase 6/4 SRM.

The SRM power output equation was presented in (Krishnan 2001). In **Equation (1)**, we determine the inner diameter of the SRM.

$$D_r = \sqrt[3]{\frac{P}{B \,.\, n \,.\, K_1 \,.\, K_2 \,.\, as \,.\, K \,.\, K_E \,.\, K_D}} \quad \textbf{(1)}$$

Where B is the flux density, as is the specific electric loading, K is the relationship with the core length, K_1 is the constant, K_2 is the ratio between the inductance values in the unaligned and aligned positions, K_E is the efficiency, K_D is the duty cycle, n is the rotor speed in rpm, and P is the power. According to (Mamede et al. 2019), the stator width (L_s) and rotor width (L_r) poles are given by **Equations (2)** and **(3):**

$$L_s = D_r \,.\, \sin\left(\beta_S / 2\right) \quad \textbf{(2)}$$

$$L_r = (D_r - 2.g) \,.\, \sin\left(\beta_r / 2\right) \quad \textbf{(3)}$$

However, to improve robustness and minimize vibration and noise, an additional factor should be considered. Consequently, the thickness value of the stator and rotor yokes should be in the following range:

$$L_s > Y_s \geq 0.5\, L_s \quad \textbf{(4)}$$

$$0.5\, L_r < Y_r < 0.75\, L_r \quad \textbf{(5)}$$

To calculate the height value of the stator and rotor poles, we need the outer and inner diameter values as well as the stator yoke thickness. Their expressions are shown respectively in **Equations (6)** and **(7)**.

$$H_s = \frac{D_s - D_r - 2Y_s}{2} \quad \textbf{(6)}$$

$$H_r = \frac{D_s - D_0 - 2g - 2Y_r}{2} \quad \textbf{(7)}$$

The 8/6 and 6/4 SRMs are studied in (Mamede et al. 2019). In this work, we update the three-phase 12/8 SRM with the same characteristics of the topologies mentioned above, changing only the number of poles and the value of polar arcs. To improve the performance of three-phase 12/8 SRM, the effect of dimensions in torque ripple and flux linkage is illustrated in Appendix A. **Figure 3** depicts the stator and rotor geometry of these machines.

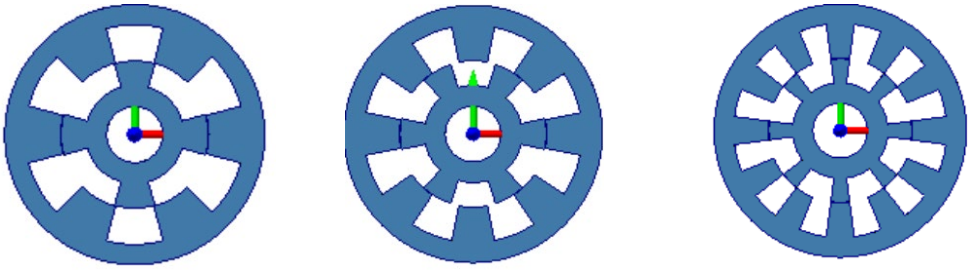

Figure 3: Structure of (a) the 6/4 SRM, (b) the 8/6 SRM, (c) the 12/8 SRM.

In order to characterize the magnetic behavior over the entire field of the three motor topologies, a computer program was developed using FEA methods. The rated power is 2.2 kW and the rated current is 10 A. Under these conditions, the three simulations had the same characteristics: design parameter, equivalent meshes, and boundary conditions. The machine parameters are assembled in **Table 1.**

Parameter	Symbol	8/6 SRM	12/8 SRM	6/4 SRM
Rotor pole angle	βr	24.5°	17°	32°
Stator pole angle	βs	22.5°	15°	30°
Stator external diameter	Ds	160mm	160mm	160mm
Rotor diameter	Dr	91.1mm	91.1mm	91.1mm
Air gap length	g	0.3mm	0.3mm	0.3mm
Stator pole height	Hr	13mm	13mm	13mm
Rotor pole height	Hs	22mm	22mm	22mm
Rotor yoke	Ys	12.45mm	12.45mm	12.45mm
Stator yoke	Yr	15mm	15mm	15mm
Shaft diameter	D0	34.5mm	34.5mm	34.5mm

Table 1: Mechanical motor parameters

2.2. SRMs Model based on FEA

An understanding of the SRM requires a detailed analysis of torques and inductances for various positions of the rotor and at different values of stator excitation currents based on FEA. So, an FEA simulation tool was used to solve the magnetic circuit to determine the magnetic fields and electromagnetic quantities of each machine. The material used to build the machine was chosen taking into account the requirements of the application (low losses, maximum performance, and high speed). Therefore, the NO20 material was set in order to have low losses at high frequencies. This simulation tool allows us to obtain data set that fully characterizes the magnetic and electromagnetic states of SRMs. Examples of this data are illustrated in **Figure 4**, **Figure 5**, and **Figure 6**. The parameters θ, i, T, and L are respectively the position, current, torque and inductance. Part of these data sets are presented in the form of three-dimensional graphs, showing the relationships between torques, inductances and currents, as well as the magnetic field distribution for the three topologies (12/8 SRM, 8/6 SRM and 6/4 SRM), respectively.

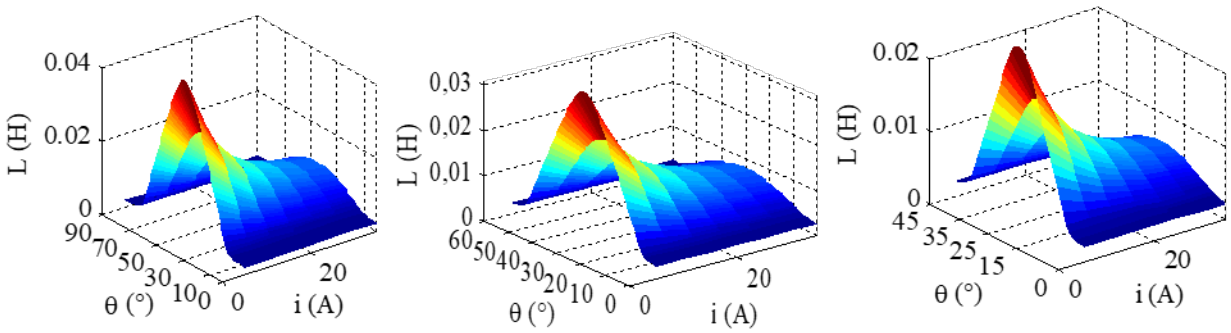

Figure 4: Inductance profile of: (a) 6/4 SRM topology, (b) 8/6 SRM topology, and (c) 12/8 SRM topology

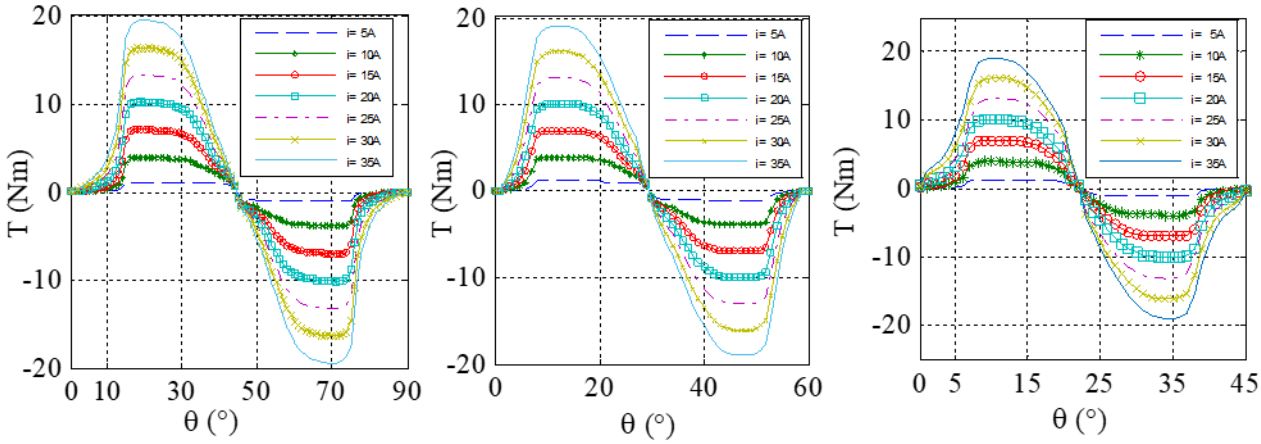

Figure 5: Torque profile: (a) 6/4 SRM topology, (b) 8/6 SRM topology, and (c) 12/8 SRM topology

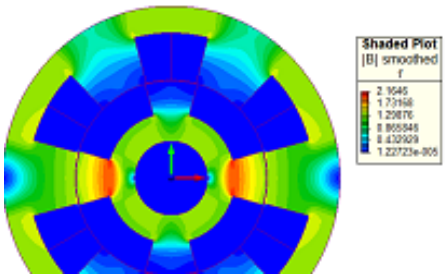

(a)

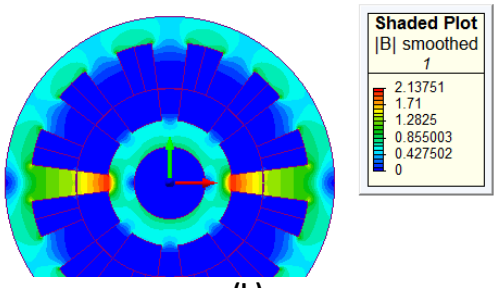

(b)

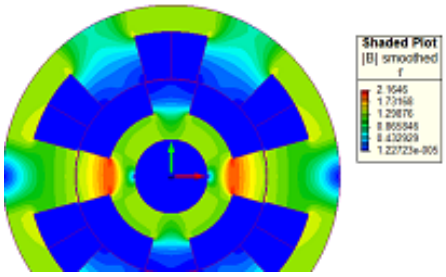

(c)

Figure 6: Magnetic field distribution for i=10A of: (a) 6/4 SRM topology, (b) 8/6 SRM topology, and (c) 12/8 SRM topology.

3. Study of Skewing Effects

The study of a radial force requires an analytical relationship between the motor design and the drive parameters. This paper will focus on the analysis of radial force distributed on the stator yoke under various skewing angles. We will discuss three methods of skewing, namely: skewed stator-SRM (SS-SRM), skewed rotor-SRM (RS-SRM), and skewed stator and rotor-SRM (RSS-SRM).

3.1. Radial Force Model

The mathematical model used to study the effect of skewing the stator, rotor, or both structures in order to reduce vibration and acoustic noise in SRMs is presented in this section. The Maxwell stress tensor method (MST) is commonly used to accurately calculate the electromagnetic torque and global forces in electrical machines (Zou et al. 2014). It is defined as follows:

$$T = \frac{1}{\mu_0}\left[(\vec{B}.\hat{n})\vec{B} - \frac{1}{2}(\nabla B^2\,\hat{n})\right] \quad \textbf{(8)}$$

Where $\hat{n}$ is the unit normal vector, μ_0 the permeability of free space, and B is flux density in magnetic circuits. According to the method of Maxwell stress, the total force is given as follows (Zou et al. 2014):

$$F = \int T\,ds \quad \textbf{(9)}$$

The total electromagnetic force F can be divided into tangential and radial components. The tangential force F_t and the radial force F_r acting on an integral surface can be described as follows:

$$F_t = \frac{1}{\mu_0}\iint B_t.B_r\,ds \quad \textbf{(10)}$$

$$F_r = \frac{1}{2\mu_0}\iint (B_r^{\,2} - B_t^{\,2})\,ds \quad \textbf{(11)}$$

Where B_t and B_r are the tangential and radial magnetic components of the flux density from the tangential direction and vertical direction, respectively. For SRM, the radial force depends on several parameters. Machine geometry, magnetic non-linearity and material properties are all included in the calculation of the radial force. For further study of the radial force in the SRM design and drive parameters, we need the basic equations and dimensions of the SRM. The air gap flux density is defined by:

$$B = \frac{\phi}{L_r.\left(D_r/2\right).\theta} = \mu_0 \frac{N.i_j}{g} \quad \textbf{(12)}$$

Where ϕ is the flux and *N* is the number of turns in one phase. The incremental input electrical energy (dW_e) and the stored energy in the magnetic field (W_s) are determined respectively by:

$$dW_e = \frac{g}{\mu_0.L_r.\left(D_r/2\right)}.\frac{\phi}{\theta}.d\phi \quad \textbf{(13)}$$

$$W_s = \frac{g}{2.\mu_0.L_r.\left(D_r/2\right)}.\frac{\phi^2}{\theta} \quad \textbf{(14)}$$

The energy balance equation is expressed as:

$$dW_e = dW_s + dW_m \quad \textbf{(15)}$$

Where dW_s is the incremental field energy and dW_m is the incremental mechanical energy, and are provided in **Equation (16)** and **Equation (17)**, respectively.

$$dW_s = -\frac{g}{2.\mu_0.L_r.\left(D_r/2\right)}.\frac{\phi^2}{\theta^2}.d\theta + \frac{g}{\mu_0.L_r.\left(D_r/2\right)}.\frac{\phi}{\theta}.d\phi \quad \textbf{(16)}$$

$$dW_m = \frac{g}{2.\mu_0.L_r.\left(D_r/2\right)}.\frac{\phi^2}{\theta^2}.d\theta \quad \textbf{(17)}$$

The tangential force is calculated by dividing the tangential torque by the rotor pole radius, as follows:

$$T_{SRM} = \frac{dW_m}{d\theta} = \frac{g}{2.\mu_0.L_r.\left(D_r/2\right)}.\frac{\phi^2}{\theta^2} = \frac{g.L_r.\left(D_r/2\right)}{2.\mu_0}.B^2 \quad \textbf{(18)}$$

The tangential force is calculated by dividing the tangential torque by the rotor pole radius, as follows:

$$F_t = \frac{T_{SRM}}{\left(D_r/2\right)} = \frac{g.L_r}{2.\mu_0}.B^2 \quad \textbf{(19)}$$

The radial force is expressed as:

$$F_r = \frac{dW_m}{dg} = \frac{1}{2.\mu_0.L_r.\left(D_r/2\right)}.\frac{\phi^2}{\theta^2} = \frac{\theta.L_r.\left(D_r/2\right)}{2.\mu_0}.B^2 \quad \textbf{(21)}$$

Figure 7(a) and **Figure 7(b)** illustrate the definition of the skewing angle for the stator and the rotor teeth. The skewing angle is the difference in angular position between the upper and the bottom corners of the pole measured from the stator center. The same definition applies to the rotor's skewing angle.

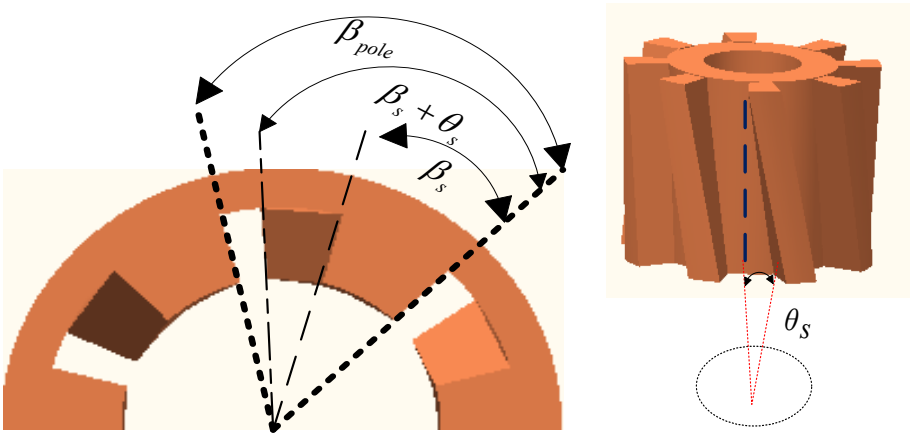

Figure 7: Definition of the skewing angle: **(a)** Stator**, (b)** Rotor.

3.2. Effect of Skewing on Radial Force

In this section, three skewing methods are studied, which are skewed-stator, skewed-rotor, and both skewed. Figure 8 shows the three motors with skewing effect. The FEA simulations will be used to demonstrate that a nonuniform air gap can produce a change of excite radial forces on the machine. The different skewing methods are presented at these points:

-The RS-SRM is composed by assembling the normal stator and rotor skewed, as shown in **Figure 8(a)**.

-The SS-SRM is obtained by assembling the stator skewed and normal rotor, as illustrated in **Figure 8(b)**.

-The RSS-SRM is composed by assembling the rotor and the stator skewed, as depicted in **Figure 8(c)**.

The three motors considered keep the same basic dimensions presented in Table 1, but with different skewing angles. The range for choosing the skewing angles is present in Equation (22), as suggested in (Yang et al. 2012). From **Figure. 7(a)**, the pole arc of the skewed stator $\beta_{S+\theta S}$, should be less than the stator pole pitch β_{pole}. The skewing angle θ_{skew} is determined by:

$$\theta_{skew} = \left(\frac{L}{\Delta L} - 1 \right) + \Delta\beta_{\theta} \quad \textbf{(22)}$$

Where L is the stack length, ΔL is the thickness of a core lamination, and $\Delta\beta_{\theta}$ is the angular distance between the two laminations that are stacked by the skewing. Therefore, the polar arc of the inclined stator $\beta_{S+\theta S}$ is expressed as follows.

$$\beta_{S+\theta_S} = \beta_S + \theta_{skew} \quad \textbf{(23)}$$

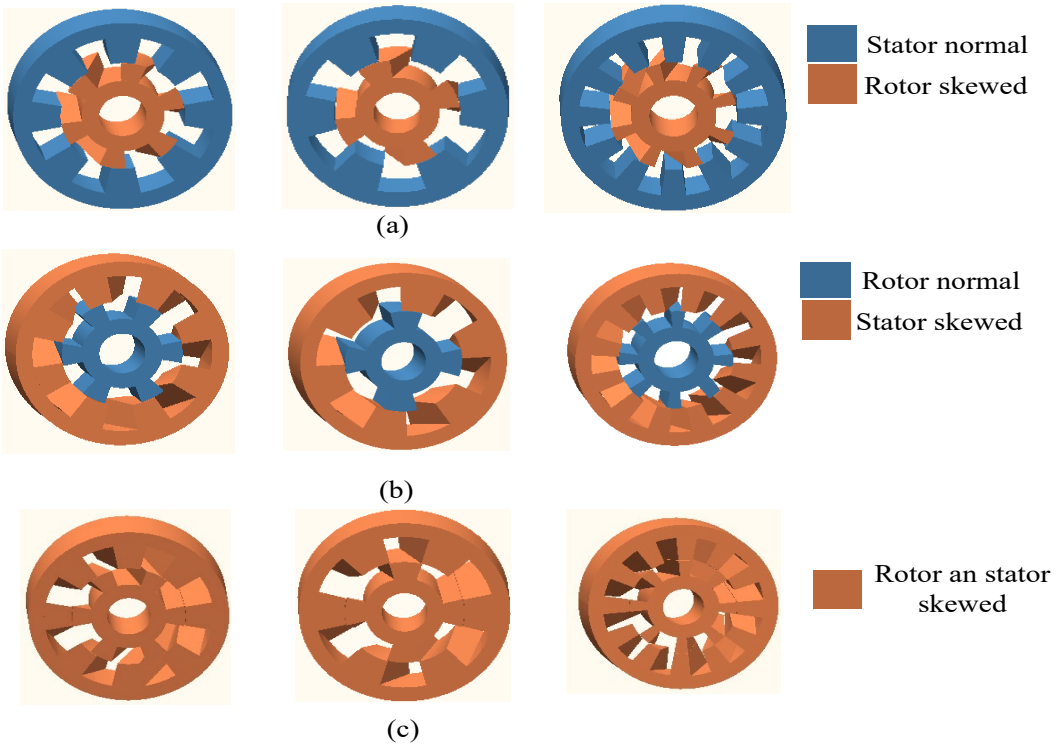

Figure 8: The SRM structures: (a) RS-SRM, (b) SS-SRM and (c) RSS-SRM.

One of the causes for vibration is the existence of a very strong magnetic attraction force between the poles of the stator and rotor, which causes the stator deformation. In fact, the deformation and radial magnetic force are distributed on the stator. In order to give some insights into this issue, we have drawn our attention to the radial force. As suggested in Hyong et al, 2013 and Chun et al. 2015 a stator pole pitch needs to be selected to analyze the radial force distributed on the stator yoke. For that analysis, we have chosen a three-phase 12/8 SRM, where the mechanical separation between adjacent stator teeth is calculated by:

$$\beta_{s-pitch} = \frac{360}{N_S} = \frac{360}{12} = 30° \quad \textbf{(24)}$$

As illustrated in **Figure 9**, the selected stator yoke for 30° is divided into 10 elements of 3° each. The middle yoke segments (i.e. Yoke 3, Yoke 4, and Yoke 5 in **Figure 9**) are aligned with the central axis of the stator tooth. With a 0° skew angle, the radial force is intensified on the yoke segments between Yoke 3 and Yoke 5. In contrast, when the skewing angle is greater, the radial force will be distributed over a large number of yoke segments. For this reason, the stator deformation can produce variations of the radial force at the stator yoke and result in a reduction of acoustic noise and vibration.

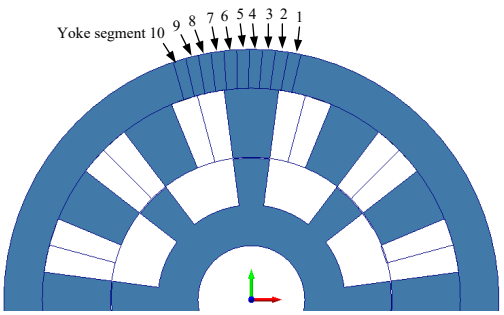

Figure 9: Stator yoke segments for the conventional stator of 12/8 SRM.

3.3. Results and Discussion

Figure 10 and **Figure 11** show comparisons of the static flux linkage and torque between the conventional SRM, RS-SRM, SS-SRM, and RSS-SRM, in the case of a 20° skewing angle. In **Figure 10:** Torque profile for the SRM, RS-SRM, SS-SRM, and RSS-SRM. (a) 6/4 SRM. (b) 8/6 SRM and (c) 12/8 SRM at 10A., compared to the conventional SRM, there is no reduction in torque production, as shown in **Table 2**.

Type of motor	Variable	Average torque (N m)	B (T)
12/8 SRM	SRM	3.68	1.56
	RSS-SRM	3.89	1.48
	RS-SRM	3.90	0.27
	SS-SRM	3.88	0.158
8/6 SRM	SRM	3.86	1.51
	RSS-SRM	3.85	1.55
	RS-SRM	3.93	2.14
	SS-SRM	3.88	2.39
6/4 SRM	SRM	3.78	1.51
	RSS-SRM	3.94	1.51
	RS-SRM	3.93	1.96
	SS-SRM	3.90	2.05

Table 2: Results of skewed teeth shapes

From **Figure 10(a)** and **Figure 10(b)**, the torque phases of the SS-SRM and RS-SRM are lagged for 18° and advanced for 18°, for 6/4 SRM and 8/6 SRM respectively. In **Figure 10(c)**, the torque of RSS-SRM compared with the traditional one advances to 2°. Visual inspection of **Figure 11** demonstrates that the flux linkage profile of the RS-SRM and SS-SRM changes more significantly than the conventional SRM.

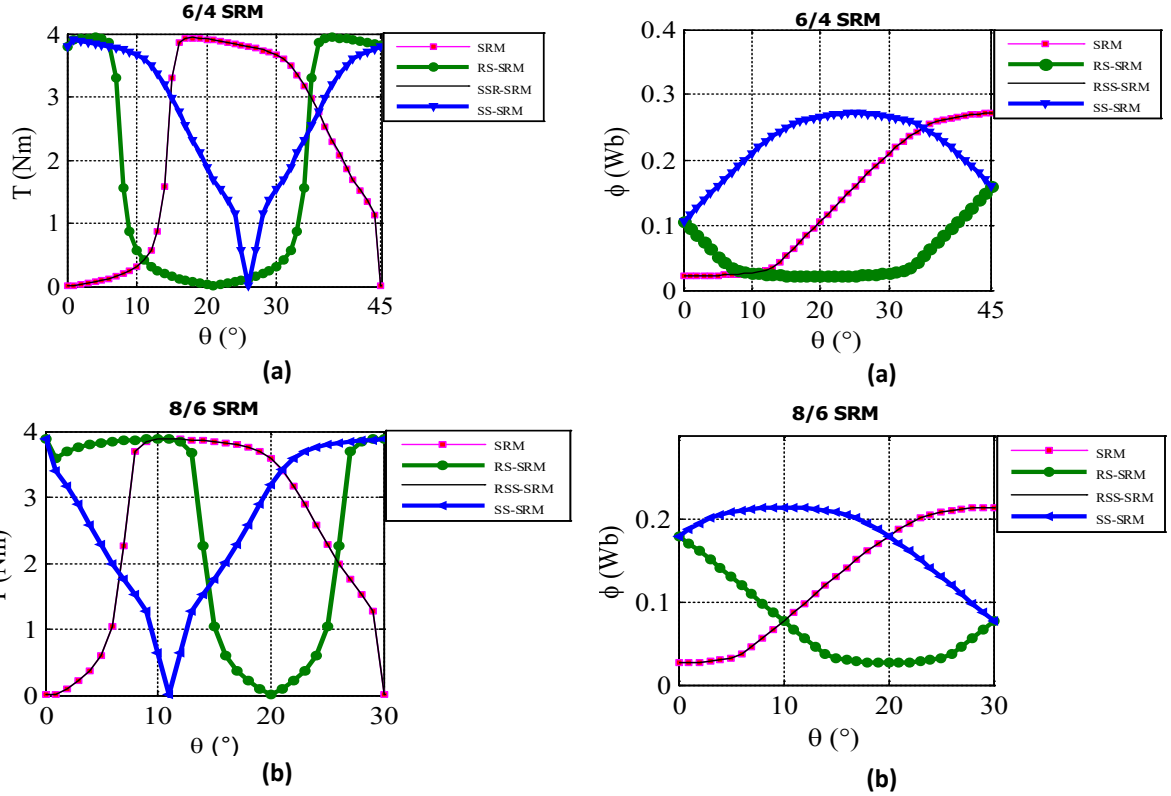

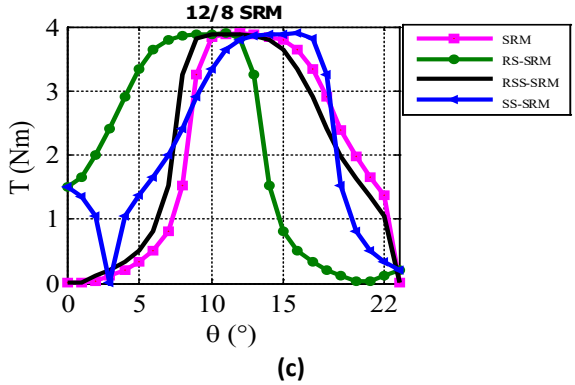

(c)

Figure 10: Torque profile for the SRM, RS-SRM, SS-SRM, and RSS-SRM. (a) 6/4 SRM. (b) 8/6 SRM and (c) 12/8 SRM at 10A.

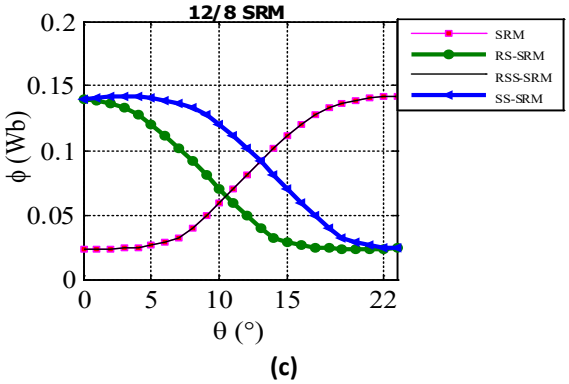

(c)

Figure 11: Flux linkage for the SRM, RS-SRM, SS-SRM, and RSS-SRM. (a) 6/4 SRM. (b) 8/6 SRM and (c) 12/8 SRM at 10A.

Moreover, the flux linkage for the different topologies has a perfect match of RSS-SRM with the traditional one. The flux phases of the SS-SRM and RS-SRM are a leading 18° and lagging 18°, for 6/4 SRM and 8/6 SRM respectively, as shown in **Figure 11(a)** and **Figure 11(b)**. For 12/8 SRM the flux phases of the RS-SRM are leading for 15°, as shown in **Figure 11(c)**. Compared to the conventional SRM, the saturation grows with the different skewing angles for the two topologies 6/4 SRM and 8/6 SRM, as highlighted in **Table 2**. In reverse, it is observed that the saturation reduces with the skew angles for 12/8 SRM. The electromagnetic characteristic of the SRM can be determined by the static torque at different current ranges and rotor positions. From **Figure 12**, we can show the torque characteristic with the skewing of stator and rotor for three motors at different currents.

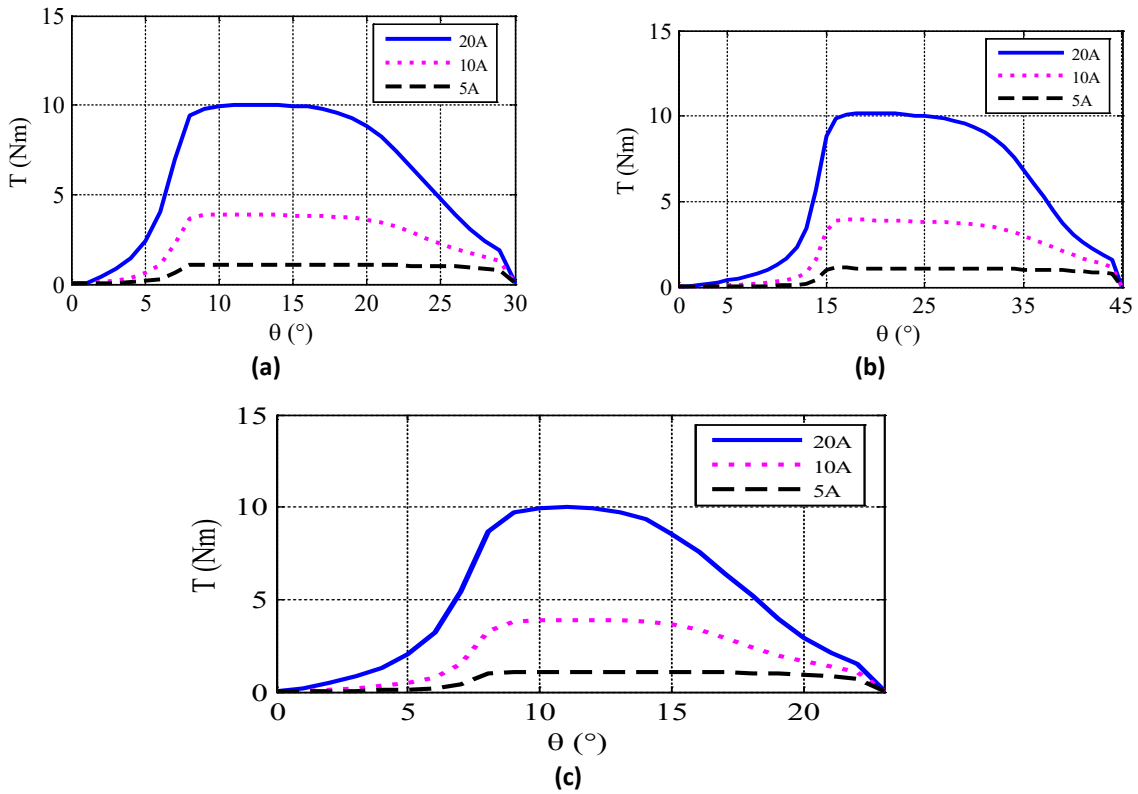

(a) (b)

(c)

Figure 12: RSS-SRM torque profile for (a) 6/4 SRM. (b) 8/6 SRM and (c) 12/8 SRM at different current.

Figure 13, Figure 14, and 15 show the comparisons of the radial force in RS-SRM, SS-SRM, and RSS-SRM, respectively with different skewing angles for the three topologies. The skew angles of the motors are chosen at 5°, 10°, 15°, and 20° respectively for this study based on **Equations 22-24**. The motors are simulated in the same operations, at the rotor alignment position of phase A with a phase current of 10A.

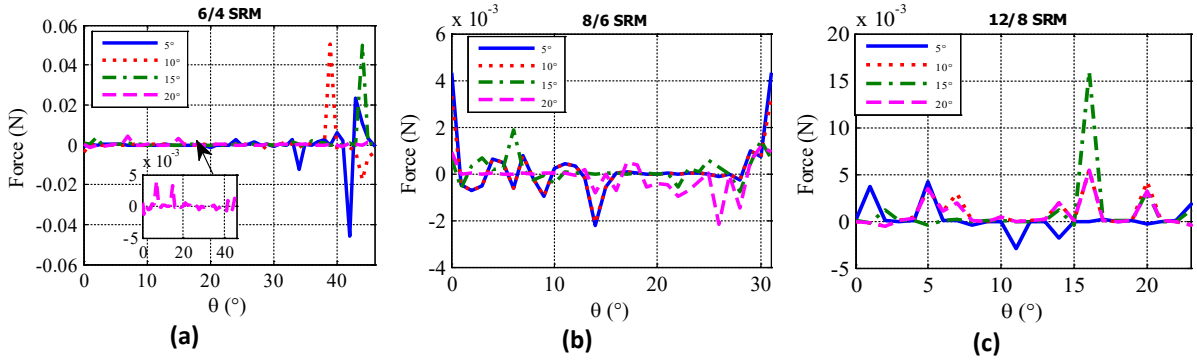

Figure 13: Radial force variation for RS-SRM with different skewing angles for (a) 6/4 SRM (b) 8/6 SRM and (c) 12/8 SRM.

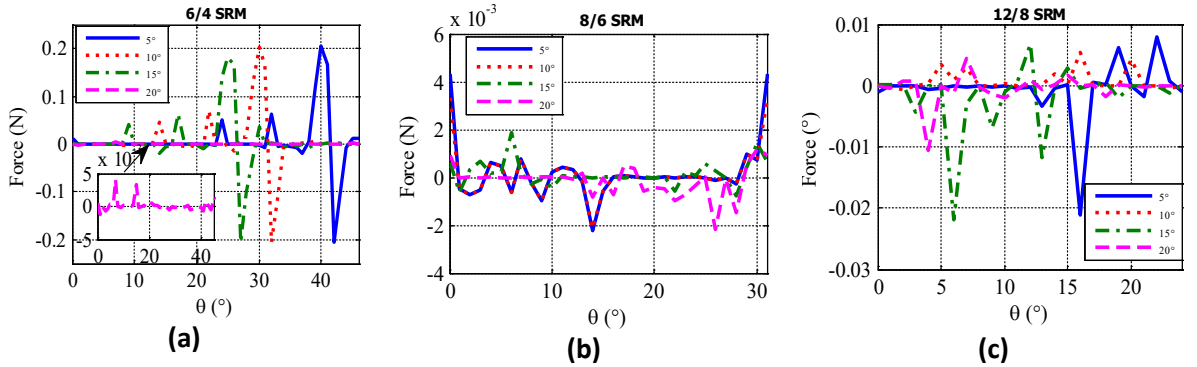

Figure 14: Radial force variation for SS-SRM with different skewing angles for (a) 6/4 SRM (b) 8/6 SRM and (c) 12/8 SRM.

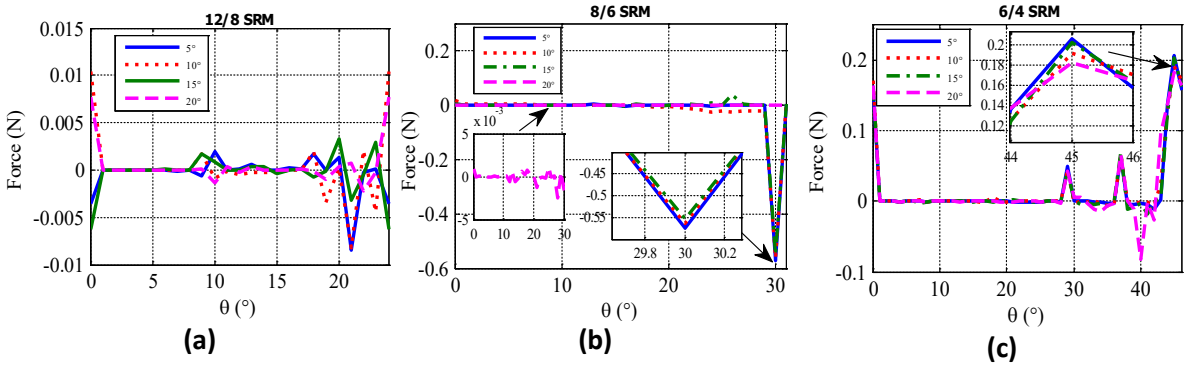

Figure 15: Radial force variation for RSS-SRM with different skewing angles for (a) 6/4 SRM (b) 8/6 SRM and (c) 12/8 SRM.

The maximum radial force of the SR-SRM, SS-SRM and RSS-SRM are all reduced when the skewed angle increases from 5° to 20° for the three topologies 6/4 SRM, 8/6 SRM and 12/8 SRM. As shown in **Figure 13**, when the rotor is skewed with different angles, the radial force varies with respect to different variation. Compared to RS-SRM 6/4 and RS-SRM 12/8, the peaks of radial force distributed on the stator yoke are much smaller for RS-SRM 8/6, as shown in **Figure 13(b)**, which can reduce the stator vibration and deformation. **Figure 14** shows the radial force with the variation of skewing angle for skewed stator (SS-SRM). The radial force is also reduced at 20° and is lower for the SS-SRM 8/6, which is similar to the force distribution in the RSS-SRM, as shown in **Figure 15**. Based on the above analysis, the acoustic noise level

and vibration are directly related to stator deformation and the numbers of poles of SRM. Our findings corroborate and are supported by the results found in Chun et al. 2015. After comparison, it is noted that: 1) The radial forces in the different topologies with RS-SRM, SS-SRM and RSS-SRM skewing are decreased with the skewing angle, and this way we could expect a reduction of vibration and noise; 2) it is also found that the vibration and noise are considerably reduced for 8/6 SRM and 12/8 SRM compared with 6/4 SRM; 3)The saturation of SS-SRM are reduced with skewing angle compared with RSS-SRM and RS-SRM; 4) It is suggested that the turn-on and turn-off angles of stator currents should be adjusted, both lagged for SS-SRM, and both advanced for RS-SRM; 5) The stator skew is more effective in attenuating vibrations than the rotor skew in SRMs, especially in SS-SRM 8/6.

4. Conclusions

This paper introduces and designs three topologies of SRM: three-phase 6/4-pole SRM, four-phase 8/6-pole SRM, and three-phase 12/8-pole SRM with different skewing methods: SS-SRM, RS-SRM, and RSS-SRM. We compared and investigated the effect of skewing on the radial force for different motors using 2D transient magnetic FEA. The flux linkage and the torque characteristics are highlighted to illustrate the performance of SR motors. The radial force distributed on the stator yoke, which is the main source of vibration, is compared under different skewing angles for the different motors. The simulation results demonstrated that the radial forces in the different topologies (RS-SRM, SS-SRM, and RSS-SRM) decreased with the skewing angle. It is found that the radial forces are considerably reduced for 8/6 SRM and 12/8 SRM compared with 6/4 SRM. The vibration and acoustic noise levels are significantly reduced by using the same skewing angle for both stator and rotor laminations without any reduction in torque production.

Appendix A

To improve torque characteristics such as reducing the torque ripples and increasing the average torque, the SRM geometry needs to be modified. In order to investigate the influence of multiple SRM geometries on electromagnetic torques, the following parameters will be modified: the air gap length g, the rotor and the stator pole arc of 12/8 SRM. **Figure 16** shows the sensitivity of the maximal torque generated by 12/8 SRM as a function of the air gap. The flux linkage value increases due to the lower magnetic flux resistance flowing from the stator to the rotor. Hence, the torque value in the aligned position to the unaligned one goes up as well. **Table 3** highlights the average torque and the magnetic field distribution (B) for the variation in the length of air gap. With an increase of 0.1 mm in the air gap, the average torque value decreases by about 17.5%.

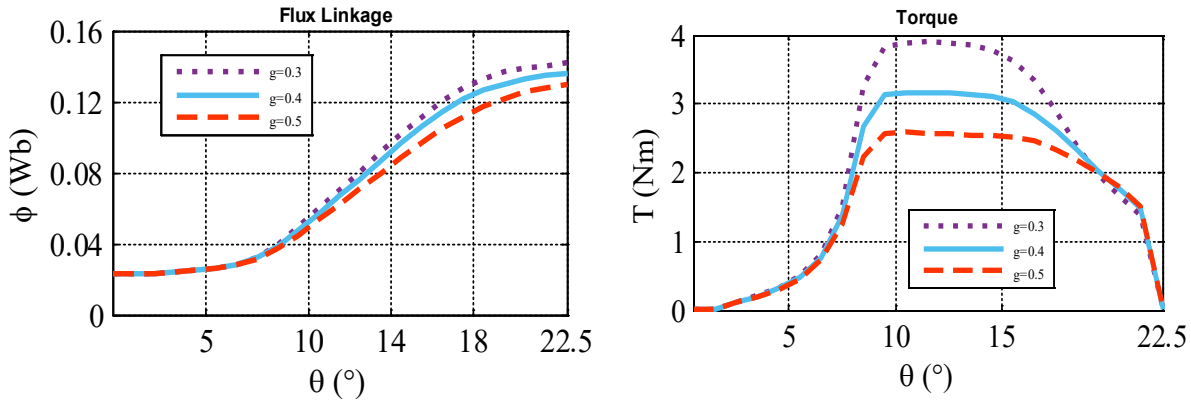

Figure 16: Influence of variation in air gap (g) on torque and flux linkage of 12/8 SRM

From **Figure 17** we can observe that the rotor pole arc has a significant influence on the shape of the torque profile and on the maximal value of the flux linkage. The flux rises in the unaligned position with the growth of βr. Furthermore, it can be observed that there is no torque production when the difference between βr and βs is very large.

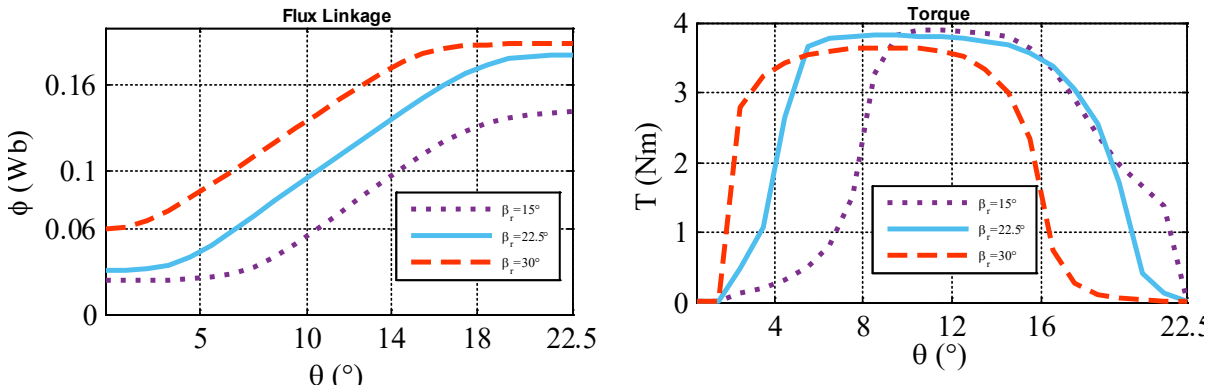

Figure 17: Influence of variation in rotor polar arc (βr) on flux linkage and torque of 12/8SRM.

It is apparent from **Figure 18 Figure 18:** Influence of stator polar arc variation (βs) on flux linkage and torque of 12/8 SRM.that the value of βs has an effective influence on the flux linkage and the torque in 12/8 SRM. The increase in the stator polar arc induces a rise in the flux value in an unaligned position, due to the larger overlap area with the rotor pole. Furthermore, the larger βs value gives a longer duration of positive torque production. From **Table 3**, it is observed that the growth of βs raises the average torque and B values.

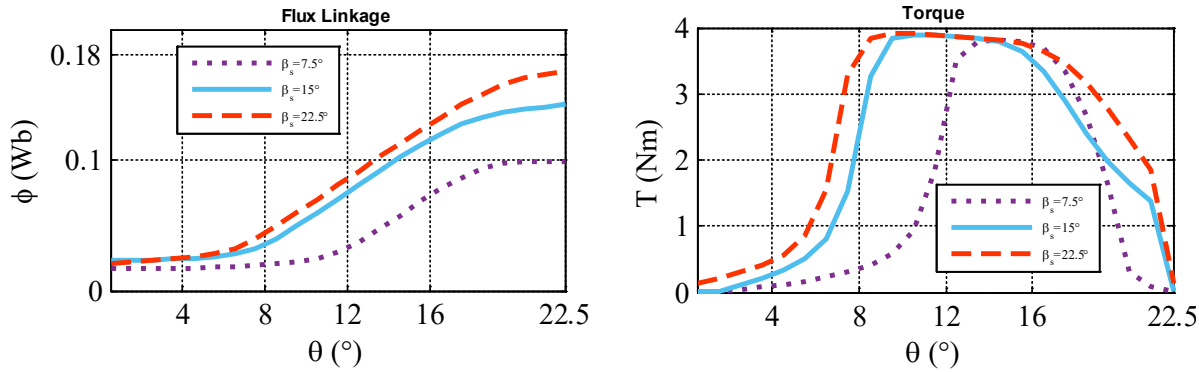

Figure 18: Influence of stator polar arc variation (βs) on flux linkage and torque of 12/8 SRM.

Variation	Variable	Average torque (N m)	B (T)
Air gap length g (mm)	0.3	3.689	2.056
	0.4	3.041	2.013
	0.5	2.525	1.835
Rotor pole arc βr	15°	3.831	1.828
	22.5°	3.781	1.782
	30°	3.566	1.725
Stator pole arc βs	7.5°	3.095	1.740
	15°	3.685	1.828
	22.5°	3.835	1.918

Table 3: Results of effect variation of 12/8 SRM.

References

Anwar, M.N., e Iqbal Husain. 2000. «Radial force calculation and acoustic noise prediction in switched reluctance machines». IEEE Transactions on Industry Applications 36 (6): 1589–97. https://doi.org/10.1109/28.887210.

Bahy, M, M Morsy Shanab, Adel Nada, e M Elbanna. 2020. «Enhancement of high-voltage ride-through of a grid-connected switched reluctance generator (srg) wind turbine using a dynamic voltage restorer based on fuzzy logic controller». Journal of Al-Azhar University Engineering Sector 15 (55): 546–59. https://doi.org/10.21608/auej.2020.87882.

Barros, Tarcio Andre dos Santos, Pedro Jose dos Santos Neto, Paulo Sergio Nascimento Filho, Adson Bezerra Moreira, e Ernesto Ruppert Filho. 2017. «An Approach for Switched Reluctance Generator in a Wind Generation System With a Wide Range of Operation Speed». IEEE Transactions on Power Electronics 32 (11): 8277–92. https://doi.org/10.1109/TPEL.2017.2697822.

Borg Bartolo, James, Marco Degano, Jordi Espina, e Chris Gerada. 2017. «Design and Initial Testing of a High-Speed 45-kW Switched Reluctance Drive for Aerospace Application». IEEE Transactions on Industrial Electronics 64 (2): 988–97. https://doi.org/10.1109/TIE.2016.2618342.

Cardenas, R., R. Pena, M. Perez, J. Clare, G. Asher, e P. Wheeler. 2006. «Power Smoothing Using a Flywheel Driven by a Switched Reluctance Machine». IEEE Transactions on Industrial Electronics 53 (4): 1086–93. https://doi.org/10.1109/TIE.2006.878325.

Chen, Hao, Guorui Guan, Guoqiang Han, e Haobiao Chen. 2020. «Fault Diagnosis and Tolerant Control Strategy for Position Sensors of Switched Reluctance Starter/Generator Systems». IEEE Transactions on Transportation Electrification 6 (4): 1508–18. https://doi.org/10.1109/TTE.2020.2997349.

Cheng, He, Lunjun Wang, Lei Xu, Xudong Ge, e Shiyang Yang. 2020. «An Integrated Electrified Powertrain Topology With SRG and SRM for Plug-In Hybrid Electrical Vehicle». IEEE Transactions on Industrial Electronics 67 (10): 8231–41. https://doi.org/10.1109/TIE.2019.2947854.

Dong, Lei, Yiyi Liu, Lulu Ling, Xiaozhong Liao, e Zhe Wang. 2017. «Design of converter topology for switched reluctance wind power generator». Em , 020037. Hangzhou, China. https://doi.org/10.1063/1.4982402.

Fathabadi, Hassan. 2018. «Plug-In Hybrid Electric Vehicles: Replacing Internal Combustion Engine With Clean and Renewable Energy Based Auxiliary Power Sources». IEEE Transactions on Power Electronics 33 (11): 9611–18. https://doi.org/10.1109/TPEL.2018.2797250.

Federal Institute of Education, Science and Technology of Goiás. Brazil, R.J. Dias, B.A. Oliveira, K.A. Silva, C.P. Alves, F.A. Ferreira, e R.R. Aguiar. 2020. «Modeling, Simulation and Comparative Study between Switched Reluctance Generator 8x6 and Switched Reluctance Generator 12x8». Renewable Energy and Power Quality Journal 18 (junho): 386–90. https://doi.org/10.24084/repqj18.340.

Ganji, B., M. Heidarian, e J. Faiz. 2015. «Modeling and Analysis of Switched Reluctance Generator Using Finite Element Method». Ain Shams Engineering Journal 6 (1): 85–93. https://doi.org/10.1016/j.asej.2014.08.007.

Gupta, Tripurari Das, e Kalpana Chaudhary. 2021. «Finite element method based design and analysis of a low torque ripple double-stator switched reluctance motor». Progress In Electromagnetics Research C 111: 191–206. https://doi.org/10.2528/PIERC21022001.

Isfahani, Arash Hassanpour, e Babak Fahimi. 2014. «Comparison of Mechanical Vibration Between a Double-Stator Switched Reluctance Machine and a Conventional Switched Reluctance Machine». IEEE Transactions on Magnetics 50 (2): 293–96. https://doi.org/10.1109/TMAG.2013.2286569.

Jayme Dias, Renato, Camille Reategui Silva, Beatriz Reis dos Santos, Charles dos Santos Costa, Augusto Fleury Veloso da Silveira, e Darizon Alves de Andrade. 2017. «Innovations on Design of 6x4 and 6x6 Switched Reluctance Generators for Increasing the Efficiency». IEEE Latin America Transactions 15 (4): 646–55. https://doi.org/10.1109/TLA.2017.7896350.

Jian Li, Xueguan Song, e Yunhyun Cho. 2008. «Comparison of 12/8 and 6/4 Switched Reluctance Motor: Noise and Vibration Aspects». IEEE Transactions on Magnetics 44 (11): 4131–34. https://doi.org/10.1109/TMAG.2008.2002533.

Krishnan, R. 2017. Switched Reluctance Motor Drives: Modeling, Simulation, Analysis, Design, and Applications. 1.a ed. CRC Press. https://doi.org/10.1201/9781420041644.

Lin, Chenjie, e Babak Fahimi. 2013. «Prediction of Radial Vibration in Switched Reluctance Machines». IEEE Transactions on Energy Conversion 28 (4): 1072–81. https://doi.org/10.1109/TEC.2013.2285165.

———. 2014. «Prediction of Acoustic Noise in Switched Reluctance Motor Drives». IEEE Transactions on Energy Conversion 29 (1): 250–58. https://doi.org/10.1109/TEC.2013.2291702.

Lu, Min-Ze, Pin-Hong Jhou, e Chang-Ming Liaw. 2021. «Wind Switched-Reluctance Generator Based Microgrid With Integrated Plug-In Energy Support Mechanism». IEEE Transactions on Power Electronics 36 (5): 5496–5511. https://doi.org/10.1109/TPEL.2020.3029528.

Mamede, Ana Camila F., José Roberto Camacho, e Rui Esteves Araújo. 2019. «Influence of Geometric Dimensions on the Performance of Switched Reluctance Machine». Machines 7 (4): 71. https://doi.org/10.3390/machines7040071.

Martinez, Clara Marina, Xiaosong Hu, Dongpu Cao, Efstathios Velenis, Bo Gao, e Matthias Wellers. 2017. «Energy Management in Plug-in Hybrid Electric Vehicles: Recent Progress and a Connected Vehicles Perspective». IEEE Transactions on Vehicular Technology 66 (6): 4534–49. https://doi.org/10.1109/TVT.2016.2582721.

Pushparajesh, V., M. Balamurugan, e Narayana Swamy Ramaiah. 2019. «Artificial Neural Network Based Direct Torque Control of Four Phase Switched Reluctance Motor». SSRN Electronic Journal. https://doi.org/10.2139/ssrn.3371369.

Sarr, Abdoulaye, Imen Bahri, Eric Berthelot, Abdoulaye Kebe, e Demba Diallo. 2020. «Switched Reluctance Generator for Low Voltage DC Microgrid Operation: Experimental Validation». Energies 13 (12): 3032. https://doi.org/10.3390/en13123032.

Somesan, Liviu-Emilian, Emil Padurariu, e Ioan-Adrian Viorel. 2013. «Two simple analytical models, direct and inverse, for switched reluctance motors». Progress In Electromagnetics Research M 29: 279–91. https://doi.org/10.2528/PIERM12103001.

Torres, Jorge, Pablo Moreno-Torres, Gustavo Navarro, Marcos Blanco, Jorge Nájera, Miguel Santos-Herran, e Marcos Lafoz. 2021. «Asymmetrical Rotor Skewing Optimization in Switched Reluctance Machines Using Differential Evolutionary Algorithm». Energies 14 (11): 3194. https://doi.org/10.3390/en14113194.

Yang, Hyong-Yeol, Young-Cheol Lim, e Hyun-Chul Kim. 2013. «Acoustic Noise/Vibration Reduction of a Single-Phase SRM Using Skewed Stator and Rotor». IEEE Transactions on Industrial Electronics 60 (10): 4292–4300. https://doi.org/10.1109/TIE.2012.2217715.

Zou, Yu, Ka-Wai Eric Cheng, Norbert C. Cheung, e Jianfei Pan. 2014. «Deformation and Noise Mitigation for the Linear Switched Reluctance Motor With Skewed Teeth Structure». IEEE Transactions on Magnetics 50 (11): 1–4. https://doi.org/10.1109/TMAG.2014.2323420.